A New Method to Model the Ionosphere across Local Area Networks

Peter F. Kolb, Xiaoming Chen, Ulrich Vollath
Trimble Terrasat GmbH

BIOGRAPHY

Peter Kolb received a Ph.D. in physics from the University of Regensburg in 2002. After postdoc research periods at the State University of New York at Stony Brook and Munich University of Technology (TUM) he joined Trimble Terrasat in August 2004. Since then he has been working on ionospheric modeling for network solutions.

Xiaoming Chen is a senior engineer at Trimble Terrasat responsible for R&D in the area of network solutions. He holds a Ph.D. in Geodesy from Wuhan Technical University of Surveying and Mapping. His primary interests are in the field of network solutions for RTK positioning systems and tropospheric modeling.

Ulrich Vollath received a Ph.D. in Computer Science from the Munich University of Technology (TUM) in 1993. At Trimble Terrasat - where he has worked on GPS algorithms for more than eleven years - he is responsible for the algorithm development team. His professional interest is focused on high-precision real-time kinematic positioning and reference station network processing.

ABSTRACT

In addition to an overall quasi-periodic 24 hour cycle, the ionosphere features many irregular disturbances. The detailed structure and dynamical evolution of the ionosphere continues to be one of the largest unpredictable factors in GNSS measurements. Across local area networks, however, the total electron content on the line of sight between the stations of a network and a given satellite is highly correlated between the stations due to the proximity of the signal rays as they propagate through the ionosphere.

In this paper we consider local area networks of 4 to 50 stations with baselines of the order of 10 to 100 kilometers. Across these networks, we characterize the ionosphere around the piercing points in terms of the average total electron content and spatial corrections to first and higher order.

To estimate the state of the ionosphere and integer ambiguities of the individual stations we process the phase measurements of the stations by means of a Kalman filter. Together with the code information and a tropospheric model for a full network solution (such as GPSNet, see Vollath et al. 2000, Vollath 2004) for reference station networks for RTK positioning, our novel approach leads to improved fixing results even during geomagnetic disturbances and for elevation angles as low as 10°. The validity of this technique is demonstrated for various networks around the globe. We find that the model correctly reproduces the expected ionospheric characteristics for all regions. While providing improved ambiguity fixing performance and reliability, the model also gives a physical description of the ionosphere throughout the day.

INTRODUCTION

Solar radiation has a strong ionizing effect on the gases of earths' ionosphere. The overall phenomenon has a periodicity of approximately 24 hours, due to the revolution of earth around its own axis. Additionally, because of irregularities in the atmosphere as well as in the solar radiation (plus some other more subtle effects) there are major irregular disturbances in the degree of ionization. These dynamical features become very vivid in movies of measurements of the electron content of the ionosphere (CODE 2005, Jakowski et al. 1997). The observed rapid evolution of the ionosphere currently defies sufficient modeling to allow its prediction to future instances. Modeling the detailed pattern of ionization therefore can at best be attempted on the fly or in post-processing.

For precise positioning using GNSS measurements, it is of greatest importance to have knowledge of the current ionospheric disturbances as they are responsible for the largest unknown term in the GNSS observation equation. The charged gases of the atmosphere act as a dispersive

medium for electromagnetic signals, such as GNSS signals. As a result, the phase of the electromagnetic wave experiences an advance shift I in its propagation, whereas the message encoded on the signal (the code) experiences a delay. The magnitude of this shift depends on the degree of ionization of the gases along the path of propagation from sender to receiver. Without precise knowledge and modeling of this error term, no precise positioning is possible.

As a function of altitude, the ionosphere shows a sharp peak at an altitude of about 350 kilometers, depending on the time of day, location of the observer, etc (Bilitza 2001). Therefore, the entire effect of the integral over the electron density along the zenith direction is often attributed to a single layer and quantified in terms of VTEC (Vertical Total Electron Content). Relevant however are mainly slanted paths through the ionosphere where an additional trigonometric factor accounts for the slanted penetration through the ionosphere TEC = $m \times$VTEC, with the mapping function $m=1/\cos(\varphi)$. and φ being the angle of penetration of the signal ray and the ionosphere (the intersection of both defines the so called pierce point). Finally the ionospheric delay/advance I (in units of meters) is in linear relation with the total electron content $I = 40.3 \text{ TEC} / f^2$ (with TEC in units of 10^6 electrons/meters^2 and f in units of Hz).

Various remedies to this problem are currently discussed, most notably attempts to gather insight in the vertical distribution of the ionospheric influence. In the Nequick 3D model (Radicella et al. 2003, Azpilicueta et al. 2003), the vertical structure of the ionosphere is parameterized in terms of profiling functions that capture the main characteristics of the ionospheric layer. Nequick 3D attempts to trace the large scale ionospheric variations across the globe. However, it does not deliver the detailed structure to obtain differential corrections across local networks, such as we propose. The same can be said for 'tomographic' models which break the ionosphere into a 3 dimensional grid that surrounds the earth (Colombo et al. 1999, Hernandez-Pajares et al. 1999a, Hernandez-Pajares et al. 1999b, Hernandez-Pajares et al. 2000). Due to limited data and computing power, such an ionospheric grid must remain rather coarse. Other modeling efforts combine the ionospheric measurements across the hemisphere visible to a satellite and apply a spherical expansion for the entire hemisphere (Liu et al. 2004). In this work, the altitude dependence is again modeled by a linear combination of orthogonal functions. The authors of this approach hope to extract a correlation in the ionosphere across distances of thousands of kilometers. Without assuming any correlations between the station, Hansen et al. (1997) trace the electron content along the signal path through the ionosphere. There have also been successful studies on the interpolation of the ionospheric residual to the approximate location of a rover within a network of reference stations with known location (Odijk 2000a, Odijk 2000b). These independent observations are interpolated to the approximate rover location to offer a correction value to the user. This is in contrast to our approach, in which correlations in the ionosphere are already exploited at the filtering level. In doing so, we employ correlations on distances of tens to hundreds of kilometers, while treating information on distances of thousands of kilometers (i.e. for the pierce points to two different satellites) as largely independent of each other. GNSS measurements are processed in a Kalman Filter to extract parameters that characterize the local state of the ionosphere across the area of a network of GNSS reference stations. The improved modeling of the ionosphere across the network area does not only deliver physical insight into the dynamical evolution of the ionosphere, but more importantly from the aspect of GNSS network solutions, it increases fixing performance and reliability, and allows more reliable calculation of correction data.

MEASUREMENTS AND MODEL FORMULATION

The crucial measurements on which we build our model are the phase measurements on wavelengths L1 and L2. In the following we assume that we have a given network of N reference stations with precisely known coordinates (x_n, y_n, z_n), $n \in \{1, \ldots, N\}$. The stations receive code and phase measurements from M satellites at coordinates (x_m, y_m, z_m), $m \in \{1, \ldots, M(t)\}$. Just as the geometry of the space segment varies continuously, also the number of visible satellites M changes with time. The separation of the reference stations is on the order of 10-100 km. The satellites are typically wider dispersed and therefore probe largely different sections of the sky. According to those geometric conditions we assume that there is a strong correlation between the ionospheric effects in between stations, but that the effects are independent in between satellites. Each satellite is treated independently of all others for the entire period where it is visible to the network. Later we will build differences between state estimates among different satellites and exploit that we can eliminate common errors in this fashion.

The true distance R between station n and satellite m is related to the phase measurement ϕ_q (where q indicates the frequency of the observation) by

$$R = \lambda_q(\phi_q + N_q) + I_q - T - MP_q - \varepsilon_{clock} - \varepsilon_q,$$

where the righthand side is greatly disturbed by nuisance parameters, in particular clock offsets in the station and satellite, leading to the term ε_{clock}. Additionally there is a frequency independent delay introduced by the troposphere T, the uncharged layer of our atmosphere, and the previously discussed advance of the wave crests due

the ionosphere I_q . MP_q is a multipath term, which results from reflections of the surroundings of the receiver and is on the centimeter level. N_q finally is the initial (theoretical) number of full wavelengths between station and satellites for a signal traveling in vacuum.

Currently the GPS system offers signals at two wavelengths λ_1 = 0.19029 m and λ_2 = 0.24421 m. Exploiting the fact that the tropospheric delay is frequency independent (as are the clock offsets and the true range between station and satellite R), we can eliminate those parameters by taking the difference of the phase measurements for the station - satellite pairs Furthermore, there is a physical relationship between the ionospheric advance for different wavelengths, which relates the effect experienced for waves of different frequencies, $I_1 / I_2 = f_2^2 / f_1^2 = \lambda_1^2 / \lambda_2^2$ an approximation that is fully sufficient for our purposes (Bassiri et al. 1992). Taking advantage of this relation and building the difference of the observation equation above for the two frequencies we obtain the fundamental 'geometry free' observation equation

$$\phi = -N + MP + I_1 + \varepsilon \ ,$$

where ϕ, N and MP now are linear combinations of the phase observation, ambiguity and multipath for different wavelengths. I_1 on the other hand is the ionospheric delay on the L1 frequency. ε is the remaining error in the measurement and the model approach.

Upon processing the measurements ϕ we seek to rapidly determine the parameters N, MP and I_1 within a consistent framework and consistent error estimates. Relevant for the determination of the integer ambiguities on wavelength L1 and L2, are the double differences of ambiguities where differences are taken once in between reference stations and once between satellites. Here however we do not assume the I_1 to be independent among the stations but assume a correlation across the network for each given satellite. This correlation is realized in terms of a Taylor expansion. As the reference point of the expansion, we use the center of the network projection with respect to a given satellite onto the ionospheric layer area (Figure 1). The pierce points of the individual stations with this satellite have relative coordinates ($\Delta\lambda_n^m$, $\Delta\varphi_n^m$) with respect to the reference point. With the concept of the mapping function introduced above, we can write the ionospheric advance as

$$I(\Delta\lambda, \Delta\varphi) = m(\Delta\lambda, \Delta\varphi)\left(\sum_{i,j=0}^{\infty} a_{i,j} \Delta\lambda^i \Delta\varphi^j \right),$$

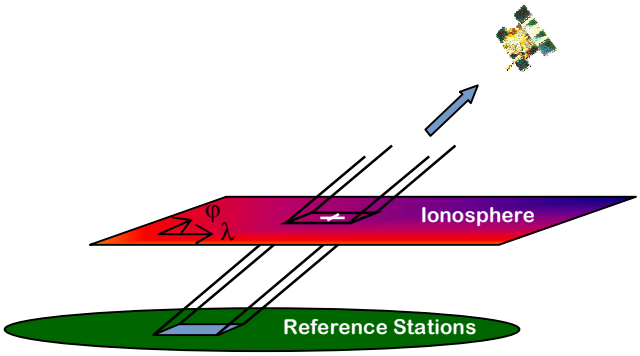

Figure 1: Illustration of the projection of a network of reference stations to the ionosphere. In reality the geometry is much more complicated as reference stations are not evenly dispersed and the ionosphere is significantly curved over the region of interest.

that is, we express it in terms of its Taylor series (or any other set of orthogonal functions, such as spherical Bessel functions). For most purposes, and as illustrated here, we can stop the expansion at first order, and introduce the terminology $a_{1,0} = a_\lambda$ and $a_{0,1} = a_\varphi$. $a_{0,0} = I_0$ is the ionospheric advance at the reference point, a_λ and a_φ are the gradients in the ionosphere in the relative coordinates. For the ionosphere at the pierce points we arrive at

$$I_n^m = m_n^m (I_0^m + a_\lambda^m \Delta\lambda_n^m + a_\varphi^m \Delta\varphi_n^m) \ .$$

For every satellite m in view we thus have the parameters (I_0^m, a_λ^m, a_φ^m) to characterize the ionosphere across the network area. Those parameters are to be estimated together with the ambiguity and multipath states. Generally, if the expansion is carried to k-th order, the number of states introduced for the ionosphere is $(k+1)(k+2)/2$ (and therefore a higher order approximation leads to slower convergence of the filtering algorithm). The remaining terms of the upper equation, m_n^m, $\Delta\lambda_n^m$, $\Delta\varphi_n^m$) are given by the geometry of the network and the position of satellite m.

RESULTS

We start to illustrate the potential of our approach by processing results from a day with strong ionosphere (March 9, 2002). The data used are obtained from a network hosted by the BLVA (Bayerischen Landesvermessungsamt) in Germany. A map of the network is displayed in Figure 2. For the following graphical illustrations we refer to data from the stations indicated in red. The typical baseline length (e.g. the baseline Augsburg-Pfaffenhofen) is about 50 kilometers.

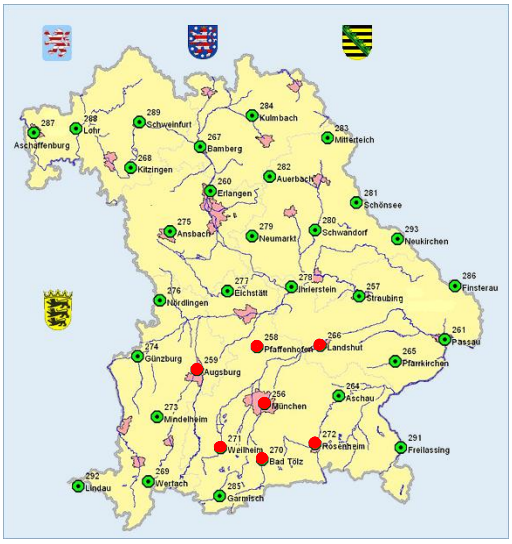

Figure 2: The SAPOS network of BLVA (Bayrisches Landesvermessungsamt) in Germany (SAPOS 2005). For the following illustrations we use a subsample of reference stations indicated in red.

Figure 3 shows the traces of the pierce points of the individual stations to the visible satellites during the course of the first half of the day in a geocentric frame. The red dots are the actual location of the sample reference stations. The dynamical evolution of the pierce points in the geocentric frame shows that the pierce points rise very rapidly over the horizon, but move very slowly once they have achieved high elevation. This also means that the mapping function changes only very slowly for high elevation satellites but changes rapidly at low elevation. This effect improves the convergence of the filter for low elevation satellites as the rapid change of the mapping function helps to disentangle the different components of the state vector in the Kalman filter.

Figure 4 shows a snapshot of a TEC Map at a certain instant of time (data from CODE 2005). Overlayed are the pierce points of the network in the solar centered reference frame, and thus constrained to latitudes from 36 to 59 degrees. Throughout the day, the pierce points travel from the left to the right, thus probing the different daily features of the ionosphere. Of course, during that time, even in the solar centered reference frame, the TEC map is not static but changes violently, as was discussed previously.

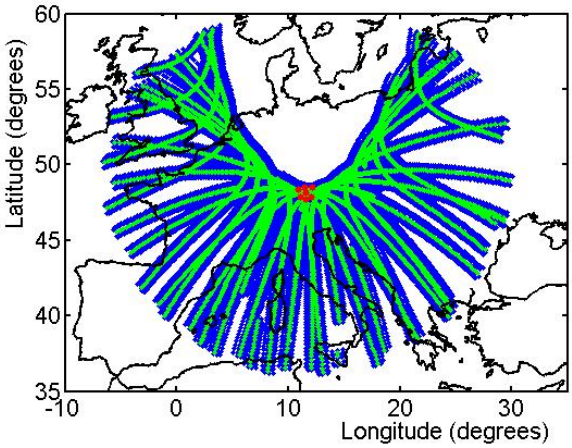

Figure 3: Pierce points of the sample network (see text) throughout a period of 12 hours in an earth fixed reference frame. Blue are the trajectories of all individual pierce points, green traces the center of the network projected to the ionospheric layer. The red dots indicate the location of the reference stations on ground.

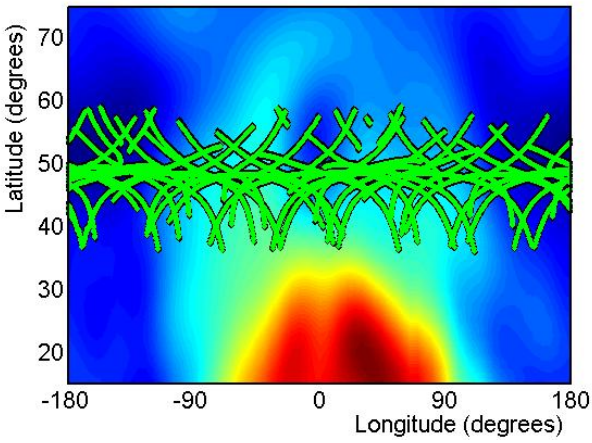

Figure 4: Pierce points of the sample network (see text) throughout a period of 24 hours in the solar centered reference frame. The trajectories of the individual pierce points are shown in black, with their geometric center in green. The color shades in the background show a qualitative example of TEC values at one instant of time, ranging from low ionization (blue) to high ionization (red).

In Figure 5 we show the state estimates returned after processing the data with a Kalman filter for the absolute ionosphere together with the gradients during a period of 24 hours. Shown are, as a function of time, the absolute ionosphere I_0 and the gradients a_λ and a_φ for satellites that are visible at that time, where different colors show

results of different satellites. The extracted parameters are in nice agreement with naïve expectations that one would have regarding the global features of the ionosphere: The ionosphere starts out very calmly at nighttime, but as the sun rises in the morning hours and illuminates the ionosphere, it ionizes more and more molecules in the atmosphere. This in turn renders the ionosphere more dispersive and induces a larger ionospheric advance, up to 15 meters on this particular day. As the pierce points probe largely different areas of the ionosphere, the plot results in a pretty broad band, and even shows one outlying result at around 13 hours local time. This is just a reflection of the rapidly changing features of the ionosphere and the correlation length of the ionosphere which is small compared to the area probed by all satellites. In the afternoon hours, when the sun declines and sets, the ionized atoms and molecules recombine, an effect that usually takes longer that the decomposition of the molecules in the atmosphere. Therefore the ionosphere approaches zero more gradually than it increased in the morning hours.

The longitudinal gradient a_λ in the panel below shows an evolution which one would also expect from the average global feature of the ionosphere. As the pierce points approach the center of highest irradiation and ionization, the gradient gradually increases, to reach a maximum before it turns to zero at the point of highest irradiation. In the afternoon hours, where the TEC decreases, a_λ is naturally negative.

For a gradual, smooth ionosphere we would expect a_φ to deliver mainly negative values throughout the day (in the northern hemisphere). As the system approaches the spot of highest ionization, one could expect the gradient to become more negative than during nighttime. This effect, however, appears to be too small to be clearly resolvable (see the third panel of the Figure 5). The figure does reflect, however, that the ionospheric conditions are more severe during daytime than at night.

Taking the Taylor expansion to second order delivers very small estimates for the second derivative. Typical values for the values of $a_{\lambda\lambda}$, $a_{\lambda\phi}$, and $a_{\phi\phi}$, are of the order of 10^{12} m^{-1}, whereas the typical order of magnitude for the gradients is about 10^{-6} or 1 mm/km. For networks with extensions of the order of 100's of kilometers this implies that the corrections from the linear terms are on the order of 10 centimeters and the quadratic contributions are about 1 cm. This increased accuracy runs clearly on the cost of the convergence time, as now more state parameters have to be estimated with the same amount of data available. It thus depends on the application whether once chooses to go beyond linear order in the modeling of the ionosphere.

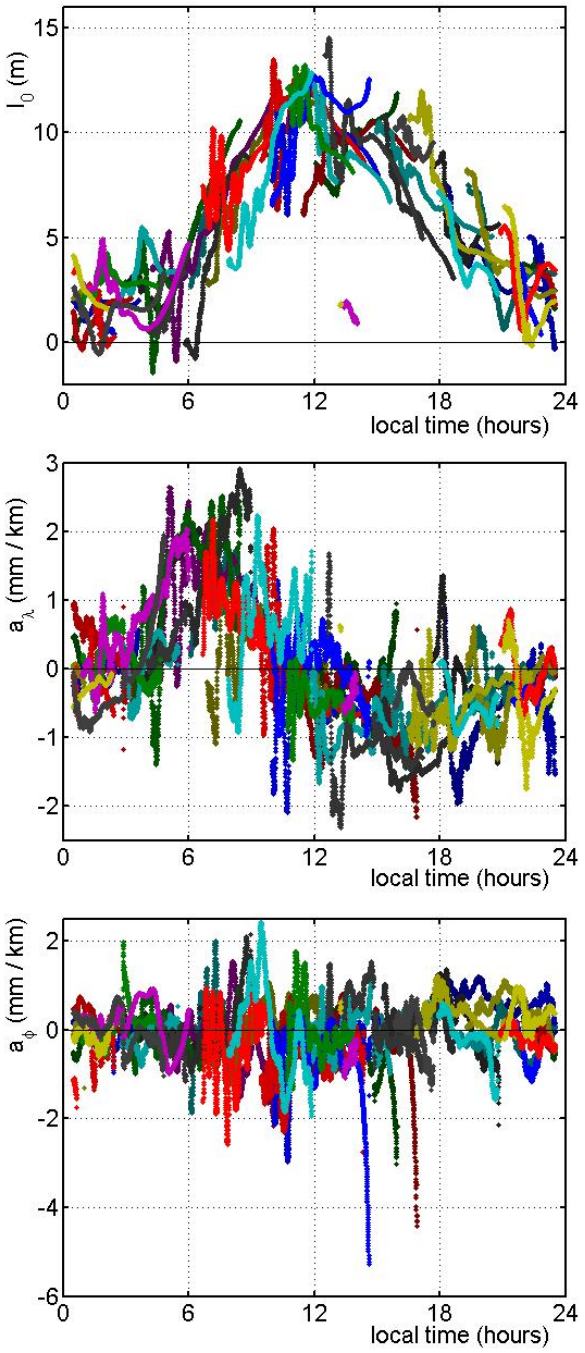

Figure 5: Upper panel: Ionospheric advance as function of time as returned by the filter for the sample network during the course of one day (different colors indicate different satellites). Middle panel: Gradient a_λ for the same calculation. Lower panel: Gradient a_φ for the same calculation.

AVAILABILITY AND RELIABILITY

To further demonstrate our method, we implement the model presented above as a part of a reference network solution (Chen et al. 2005) to resolve integer ambiguities. The following calculation uses the dataset discussed above with an elevation cutoff of 10 %. Figure 6 compares the number of tracked satellites and the number of fixed satellites for hours 6 to 15. During that period, the ionospheric advance exhibits a very strong increase and therefore presents the most challenging time of day to model. While the homogene ionosphere (zeroth order Taylor expansion) delivers unsatisfactory fixing performance, the first order calculation results in very short fixing times. The lower panel of Fig. 6 shows the number of unfixed satellites in a comparison of zeroth and first order calculation.

We continue to process data from several network stations around the globe and different seasons of the year to account for regional and seasonal differences. The data are generally from a period of strong solar and ionospheric activity, in the years 2002-2003. Table 1 gives a summary of the percentage of resolved ambiguities for satellites with elevation greater than 10 degrees. All results were obtained with the same set of parameters that govern the detailed behavior of the processing Kalman filter, such as process noise, correlation lengths and correlation times. It is truly remarkable that the very different systems can be described with great success simultaneously, without requiring any retuning of the parameters. However, still higher performance rates can be obtained by adapting to regional specifics, such as higher noise input on the ionospheric gradients for networks close to the equator, as for Japan.

It is interesting to note that the small sized network (Ruhrgas with only four stations) delivers best results for the zeroth order approximation (i.e. a homogene ionosphere). For such small networks, apparently the modeling of gradients is not yet required. If gradients are modeled, more states have to be estimated with the same amount of data available, and the states take longer to converge, leading to lower fixing rates. However, for larger networks it becomes essential to model gradients to obtain full reliability. None of the results to first or second order delivered wrong fixes, whereas wrong fixes are obtained for larger networks in the zeroth order approximation. Many more data samples have been processed (not shown here), all with 100 % reliability. Except for a few cases, the difference in fixing performance between first and second order are very small for the results displayed. Taking the fixing performance as criterion, the calculation to first order suffices to obtain improved performance.

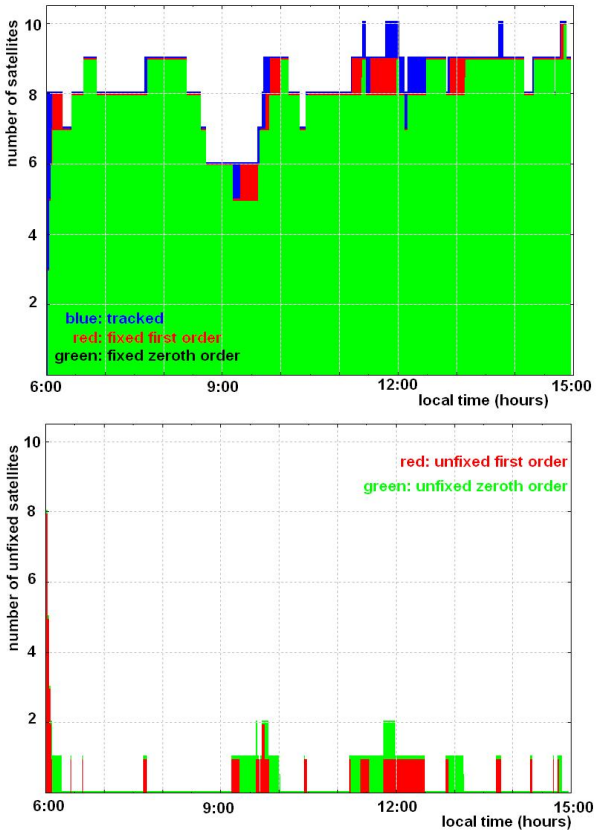

Figure 6: Upper panel: Number of tracked satellites (blue) during period of strongest increase of the ionosphere. Shown in green is the number of fixed satellites applying the previous model to zeroth order (homogene ionosphere across the network), shown in red is the number of fixed satellites applying the model to first order.
Lower panel: Number of unfixed satellites for zeroth and first order calculation. Results to second order are essentially identical to the displayed results of first order.

SUMMARY

We have presented a novel method to extract characteristic parameters to describe the ionosphere across a network of reference stations using GPS measurements. The main concept of the model is an expansion of the ionospheric delay in terms of a series of orthogonal functions across the area spanned by the piercing points of the ionosphere. The piercing points with respect to a given satellites are thus assumed to be highly correlated, whereas the ionosphere at pierce points with respect to different satellite are considered as fully independent of each other.

network	stations extension	day/ year	fixing performance (%)		
			zeroth order	first order	second order
Ruhrgas	4	155/02	98.70	96.26	94.78
Germany	70x60	156/02	98.91	96.44	95.73
GSI	7	019/02	96.21	97.68	97.65
Japan	75x100	020/02	96.68	97.73	97.58
Thüringen	22	324/03	95.60	97.89	97.99
Germany	200x165	325/03	99.48	99.51	99.51
NRW	22	009/03	98.33	98.46	98.47
Germany	250x150	010/03	98.35	98.58	98.56
Swisstopo	29	213/02	98.11	98.52	98.57
	310x210	214/02	98.15	98.23	98.24
ascos	21	228/02	98.42	98.84	98.85
Germany	250x350	229/02	96.74	99.11	99.13
BLVA	35	290/03	98.98	99.06	99.05
Germany	260x330	291/03	98.80	98.99	98.98
ascos	28	113/03	98.39	99.03	99.23
	250x350	114/03	98.03	99.29	99.29

Table 1: Fixing rates of GPS satellites for different networks. The second column gives the number of stations in the network, together with the approximate extension of the network (in km x km). Results are shown for the calculation to zeroth, first and second order for different days.

We have demonstrated that this model delivers physically reasonable output and reflects the overall characteristics of the ionosphere during the period of a day. Furthermore we have shown that this method leads to improved processing of the measurements. Within a network solution, we have obtained results for networks at different locations and very different sizes. Without adjusting parameters of our calculation to account for regional, seasonal or solar cycle specific peculiarities, very high performance for all networks with full reliability was achieved.

REFERENCES

Azpilicueta F., Nava B., Coisson P., and Radicella S.M. (2003), Optimized NeQuick Ionospheric Model for Point Positioning, *Proceedings GNSS 2003, Japan*.

Bassiri S. and Hajj G.A. (1992), Modeling the Global Positioning System Signal Propagation Through the Ionosphere, *TDA Progress Report 42-110, August 1992.*

Bilitza D. (2001), International Reference Ionosphere 2000, *Radio Science 2 (36) 2001, pp 26,*. http://nssdc.gsfc.nasa.gov/space/model/ionos/iri.html

Chen X., Deking A., Landau H., Stolz R., and Vollath U. (2005), On the Influence of Different Network Correction Formats on Network RTK Performance, *ION GPS 2005 Long Beach.*

CODE (2005), Center for Orbit Determination in Europe, Global Ionosphere Maps Produced by CODE, http://www.aiub.unibe.ch/ionosphere.

Colombo O.L., Hernandez-Pajares M., Juan J.M., and Sanz J. (1999), Resolving Carrier-Phase Ambiguities on the Fly, at more than 100 km from nearest Reference Site with the Help of Ionospheric Tomography *ION GPS 1999, Nashville.*

Hernandez-Pajares M., Juan J.M., and Sanz J. (1999a), New Approaches in Global Ionospheric Determination using Ground GPS Data, *Journal of Atmospheric and Solar Terrestrial Physics (**61**) 1999, pp 1237*.

Hernandez-Pajares M., Juan J.M., Sanz J., and Colombo O. (1999b), Precise Ionospheric Determination and its Application to Real-Time GPS Ambiguity Resolution, *ION GPS 1999, Nashville.*

Hernandez-Pajares M., Juan J.M., Sanz J., and Colombo O. (2000), Application of Ionospheric Tomography to Real-Time GPS Carrier Phase Ambiguities Resolution, at Scales of 40–100 km and with High Geomagnetic Activity, *Geophysical Research Letters, 13 (27) 2000, pp 2009.*

Jakowski N., Schlüter S, and Jungstand A. (1997), Total Electron Content of the Ionosphere during the Geomagnetic Storm on 10 January 1997, http://www.kn.nz.dlr.de/ionos/Storm/storm.html.

Liu Y. and Gao Y. (2004), Development and Evaluation of a New 2-D ionospheric Modeling Method, *Navigation 4 (51) 2004, pp 311*.

Odijk D. (2000a), Improving Ambiguity Resolution by Applying Ionosphere Corrections from a Permanent GPS Array, *Earth Planets Space 10 (**52**) 2000, pp 675*.

Odijk D. (2000b), Weighting Ionospheric Corrections to Improve Fast GPS Positioning Over Medium Distances, *ION GPS 2000, Salt Lake City.*

Radicella S.M., Leitinger R., Nava B., and Coisson P. (2003), A Flexible 3D Ionospheric Model for Satellite Navigation, *Proceedings GNSS 2003, Japan*.

SAPOS (2005), Webpages addressing the Satellite Positioning Service of the Bayerisches Landesvermessungsamt at http://www.geodaten.bayern.de/bvv_web/blva/

Vollath U., Bücherl A., Landau H., Pagels C., and Wagner B. (2000), Long-Range RTK Positioning Using Virtual Reference Stations, *ION GPS 2000, Salt Lake City*; Multi-Base RTK Positioning Using Virtual Reference Stations, *ION GPS 2000, Salt Lake City*.

Vollath U. (2004), The Factorized Multi-Carrier Ambiguity Resolution (FAMCAR) Approach for Efficient Carrier-Phase Ambiguity Estimation, *ION GNSS 2004, Long Beach.*